

Interface Friction and Deformation Kinematics in Metal Compression with Sticking Friction

D.K. Dasgupta

Friction at the die-metal interface results in nonuniform deformation in metal compression. With sticking friction, the plastic flow mechanism becomes extremely complex, and the force and energy requirements are higher compared to frictional compression. Earlier research, which had some limitations, enables evaluation of the forming load in metal compression involving sticking friction. In the present article, critical analysis has been made regarding frictional behavior at the real contact areas to propose a more realistic estimation of frictional constraints. For this purpose, available inferences in specific areas of metal forming, concerning fundamental concepts of friction and the influence of interface shear stress, bulk deformation, etc., on frictional behavior, have been used and modified as required. Also, a rational deformation kinematics has been proposed, assuming velocity discontinuity at every point within the flow field. The proposed estimation of friction and plastic flow kinematics yields results in line with the published experimental findings and the corresponding slip-line field solutions.

1. Introduction

FRICTION at the die-metal interface has a significant effect on the load requirement and formed metal geometry in metal compression. With friction, the deformation process is nonhomogeneous, and plastic flow kinematics become extremely complex. Also, the load and energy requirements are higher compared to frictionless forming. Figure 1(a) shows uniform flow of metal in the case of frictionless compression. Figure 1(b) indicates the associated redundant deformation, if friction exists at the interface.

A considerable amount of information has been reported in the past three decades concerning deformation mechanisms and frictional behavior occurring at the interface in various metalforming operations. Attempts continue to predict and explain more precisely the frictional constraints and their effect on the plastic flow kinematics under the condition of sticking friction. Several theories and analytical methods were developed using some pertinent assumptions to evaluate forming load and energy. Some of the methods that were developed earlier considered either a constant friction coefficient or a constant shear stress at the interface. Subsequent developments assumed a combination of a frictionless zone and a constant shear stress zone at the interface to predict more accurate results in the case of sticking friction.

Various analytical techniques to determine upsetting load, considering friction or without friction, are:

- Slab-force balance method
- Upper bound slab-energy method
- Traditional upper bound method
- Combined upper bound slab-energy method and traditional upper bound method
- Slip-line field theory

The fundamental assumptions and process evaluation of these methods have been discussed extensively in the available literature for various forming operations.[1-8] Examples of extensive application of these theories and techniques to determine load and torque under different conditions of hot metal rolling have been referenced.[9-14] Comparison of the results obtained from the various methods listed above for compression of metal with sticking friction is shown in Fig. 2.[1]

The fundamental concepts and the role of interface friction relating to bulk deformation have been studied on the microlevel in the areas of sheet-metalforming, namely stretch forming and deep drawing. Exhaustive references on interface contact geometry and its bearing on the tribological behavior of the interface are available in the literature. In the first section of this article, a brief review of the fundamental concepts concerning interface friction in metalforming has been made. In the second section, sticking friction applied to metal compression has been critically studied. A two-stage deformation model, along with a suitable stress field, has been proposed at real contact areas to enable a more realistic estimation of frictional constraints at the interface. In the last section, the plastic flow mechanism in metal compression has been analyzed, taking

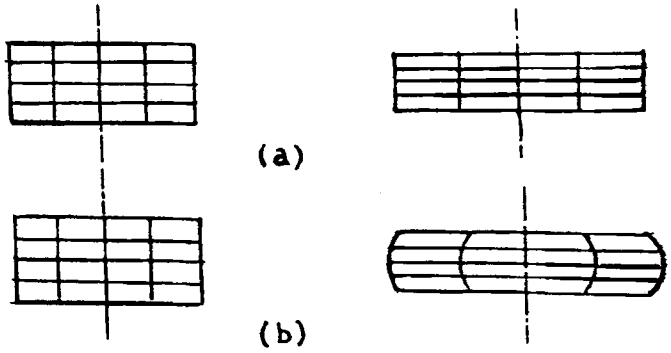

Fig. 1 Deformation in metal compression. **(a)** Homogenous deformation. **(b)** Redundant deformation caused by sticking friction at the die-metal interface.

D.K. Dasgupta is with Metallurgical & Engineering Consultants (1) Ltd. Durgapur, India.

into consideration the effect of sticking friction. More rational flow kinetics have been proposed in cases of plane-strain and axisymmetric compression. The velocity fields satisfy certain assumed boundary conditions and reject the possibility of metal flow as solid blocks or the true existence of any dead metal cap in the flow field. The results obtained from the proposed analysis have been presented for comparison and discussion.

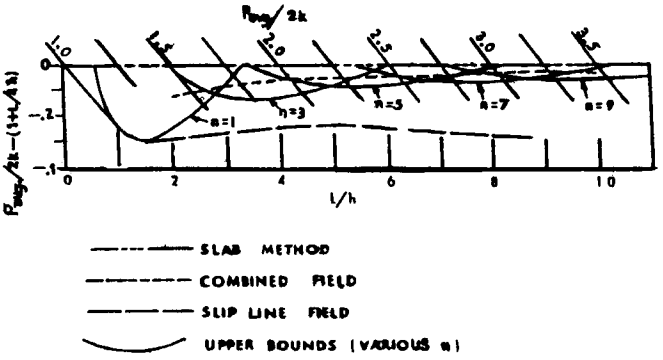

Fig. 2 Comparison of yield pressures for plane-strain compression evaluated by various analytical methods.

2. Fundamental Concepts Concerning the Role of Friction in Metal Forming

Interface frictional behavior at the die-metal interface in specific areas of metalforming has been investigated and studied in detail by many researchers in the past. The fundamental concepts concerning the role of friction and the factors influencing frictional constraints are briefly discussed below.

Frictional characteristics at the die-metal interface are dependent on the state of stress and deformation at the real contact zones, the latter being influenced by factors like bulk deformation of the metal, gross or microsliding at the interface, etc. The die and the metal surfaces contain hills and valleys of various heights that are significant in terms of an atomic scale. When the die and the metal surfaces are brought in contact, they meet at high spots, known as asperities. The simplified and exaggerated views in Fig. 3(a) illustrate this phenomenon. The asperities on the die surface are usually much harder and less pronounced than those on the metal surface. For practical purposes, however, the die surface can be considered to be "smooth" compared to the "rough" metal surface.

The geometric properties of the surface textures of the contacting bodies normally play a significant part in frictional behavior. Surface roughness is usually measured by means of stylus instruments, and a number of parameters can be quantified from the topography charts thus obtained. A detailed account of the surface texture measurement parameters and their functional importance has been given by a number of researchers.

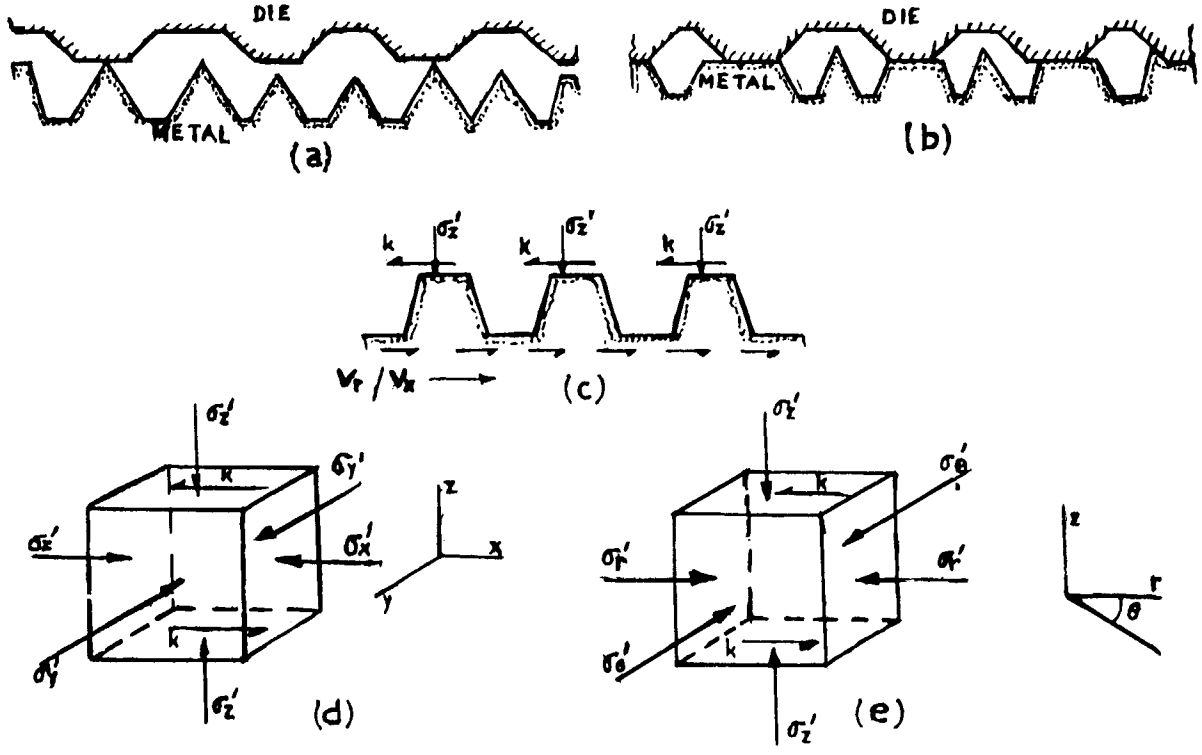

Fig. 3 Deformation and stresses at asperity peaks. (**a**) Peaks and valleys on metal surface. (**b**) Primary asperity deformation model. (**c**) Asperities at the onset of bulk deformation. (**d**) Stresses at asperity peaks for plane-strain compression. (**e**) Stresses at asperity peaks for axisymmetric compression.

Adequate references on contact geometry and its effect on the tribological behavior are also available in the literature.[15-23]

The initial actual area of contact is brought about by deformation at the tips of the highest asperities. Asperity deformation mechanics can be considered as the inverse of indentation of a semi-infinite block with a flat punch. Tabor showed that, in the absence of gross deformation or sliding (*i.e.*, normal loading), the asperity collapse pressue, P_m, is approximately 2.8 to 3.0 times the compressive yield stress of the bulk metal, and as such, the number and the total area of asperity contacts are decided by the level of the applied load, under normal contact loading.[24] This necessitates substantial deformation or collapse of the asperities initially in contact, growth in individual junction areas, and contact with and deformation of more asperities. The combined areas of contact at all asperity junctions, under normal loading, can therefore be given as:

$$a_o = \frac{F}{P_m} \qquad [1]$$

where a_o is the combined real contact area, and F is the applied load.

Growth in the contact area further increases if a shear stress acts on the face of the asperity junction in addition to the applied load, which may occur in micro- and gross sliding during deep drawing or stretch forming operations. Tabor introduced a generalized yield criterion to describe asperity deformation mechanics under externally imposed tangential sliding:[25]

$$\tau^2 + \lambda \tau^2 = \tau_m^2 \qquad [2]$$

where P' is the modified contact pressure at real contact zones; τ' is the shear stress at real contact zones; and λ is a constant that depends on the work-hardening properties of the softer metal in contact.

The coefficient of friction μ is

$$\mu = \frac{\tau'}{P'} \qquad [3]$$

If a is the combined real contact area in the presence of shear stress at the interface, Eq. 2 (from Tabor) can be rewritten in the form:

$$1 + \lambda \mu^2 = \left(\frac{a}{a_0}\right)^2 \qquad [4]$$

Tabor's generalized equation (Eq 2), however, does not take into consideration the bulk deformation of the metal. Adequate research in the past, concerning deep drawing and stretch forming, reported that planar plastic deformation in the substrate leads to considerable roughening of the free surface of the metal. Grains under movement, at or near the free surface, remain relatively unworked in spite of substantial bulk straining. The presence of constraint at the metal surface in the form of a hard punch or tool surface promotes an almost complete strain transfer from the bulk to the surface layer, seriously affecting the asperity collapse mechanism. Traces on the surfaces in contact with the polished punch in the absence of lubrication demonstrate further junction growth and an extensive degree of asperity flattening. Accordingly, Tabor's equation (Eq 2) was modified to consider bulk tensile deformation:[26-29]

$$\tau^2 + \nu s^2 + \delta s \tau' + \lambda \tau^2 = \tau_m^2 \qquad [5]$$

where s is the generalized bulk stress, and ν and δ are constants that depend on the actual bulk deformation in the contact zone.

Equation 5 shows that both tangential micro- or gross sliding at the interface and bulk deformation cause a decrease in asperity collapse pressure, with a corresponding increase in real contact areas in sheet-metal-forming. This aspect was well established in the model asperity tests reported by Fogg.[28]

3. Interface Friction Applied to Metal Compression

In the compression process, the interface frictional characteristics at real contact areas do not behave in the same manner as in sheet-metal-forming due to the difference in deformation modes of the bulk metal. In sheet-metal-forming, the tool or punch pressure converts to stretch in the metal. Bulk tensile strain is transferred to the interface surface layer, associated with micro-sliding, and as a result, the asperity collapse pressure decreases. In the compression process, the metal under die pressure is forced to flow outward laterally. The bulk strain transferred to the interface surface layer would be compressive in nature, presumably associated with micrco-sliding at the initial stage. The asperity collapse pressure is therefore likely to increase. In the following paragraphs, an attemt has been made to explain the influence of bulk deformation and plastic flow on the frictional characteristics in the compression process. The fundamental concepts and behavior of friction, as discussed earlier, have been used and modified as required to derive the local and average friction coefficient, contact pressures, etc.

3.1 *Primary Asperity Deformation and Junction Growth*

Asperity collapse and junction growth at the interface before the onset of gross deformation have been termed primary asperity deformation and junction growth. This phenomenon takes place under normal loading conditions, *i.e.*, in the absence of tangential sliding and bulk deformation, as stated before. For the purpose of analysis, the value of critical collapse pressure, P_m, is assumed to be 2.9 σ_0. Figure 3(b) shows a model of primary asperity deformation.

3.2 *Secondary Asperity Deformation and Junction Growth*

At the onset of bulk plastic yielding, primary junction growth at the asperity peaks is seized. Instantaneously, a shear stress equal to k, the yield stress in pure shear, is developed at the real contact areas to oppose lateral plastic flow, as an immediate influence of the bulk strain transfer to the interface. Asperities thus in contact are put to severe shear deformation (Fig. 3c). Soon, complete transfer of the strain level of the substrate to the interface surface layer takes place, resulting in further junction growth and extensive asperity flattening. The surface texture thereafter, as seen in sheet-metalforming, undergoes very little change. This part of the frictional development at the

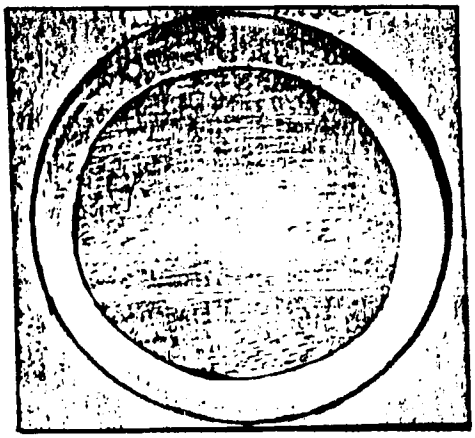

Fig. 4 Surface appearance of a disc subjected to compression.[1]

interface has been termed as secondary asperity deformation and junction growth.

From kinetics, it may be seen that the velocity of lateral plastic flow increases from the center toward the edge. It may therefore be argued that strain transfer and secondary asperity growth and flattening take place more quickly near the edge compared to the inner part of the metal surface. Almost the entire metal surface at the edge comes in contact and sticks to the die surface. Full sticking at the edge subsequently arrests any deformation, and micro-sliding at the adjacent surface elements inward. Gradually, grains on the entire surface layer become stagnant, and no further strain transfer to the interface or change in surface texture can take place. The complete metal surface thus becomes locked to the die surface. At the center, subsurface plastic flow is absent, and therefore, shear stress or the friction coefficient at the central contact zone must be equal to zero.

As compression continues and the metal expands laterally, material that was originally on the side of the specimen folds onto the die surface, increasing the total contact area. Based on the above analysis, it may be predicted that full sticking also should occur at the newly generated surface beyond the original edge. Figure 4 shows the surface appearance of a disc subjected to compression.[7] The outer annular-like band was originally part of the cylindrical surface, and sticking occurred there.

The foregoing discussions enabled a few valuable assumptions to be made regarding frictional behavior after total asperity flattening and contact growth:

- Combined real contact areas and frictional resistance are at a maximum at and near the edge of the metal specimen, and full sticking occurs there.
- At the interior, secondary junction growth and frictional stresses are progressively less towards the center.
- At the onset of bulk plastic flow, total frictional stresses between the center and the edge, along a narrow strip of metal surface, reach a critical value, determined by the yield shear stress k and yield criterion at individual asperity peaks, and do not increase further at subsequent stages.

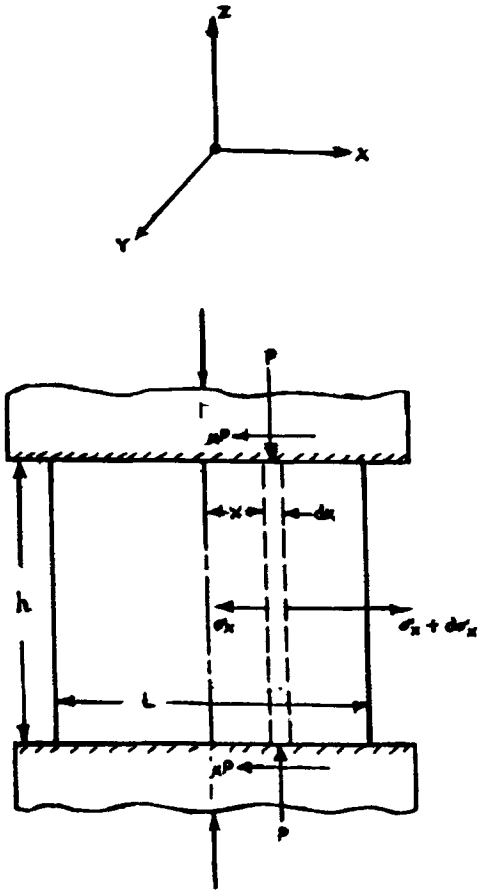

Fig. 5 Schematic of slab-force analysis in plane-strain compression with sticking friction.

However, no prediction regarding distribution of frictional stresses at the onset of gross deformation is possible, because the distribution of real contact zones at this stage solely depends on the initial topography of the metal surface.

4. Interface State of Stress and the Average Friction Coefficient at the Onset of Bulk Deformation

The interface state of stress and the average friction coefficient at the onset of bulk deformation can be evaluated in cases of plane-strain and axisymmetric compression as follows.

4.1 *Plane-Strain Compression*

Referring to Fig. 5 the proposed state of stress at any point on the asperity peak at the onset of bulk yielding is shown in Fig. 3(d). From the discussions:

$$\sigma_z' = P_m$$

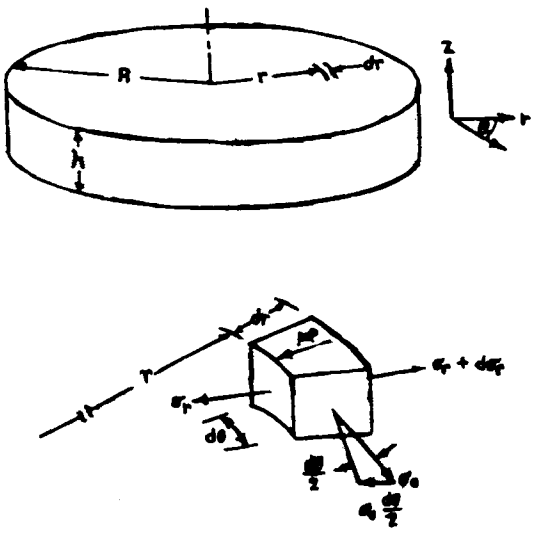

Fig. 6 Schematic of slab-force analysis in axisymmetric compression.

$$\tau'_{xz} = k$$

$$\tau'_{xy} = \tau'_{yz} = 0$$

where σ'_x, σ'_y, and σ'_z are orthogonal compressive stresses, and τ'_{xy}, τ'_{yz}, and τ'_{xz} are shear stresses. The von Mises yield criteria for secondary asperity deformation is

$$(\sigma'_x - \sigma'_y)^2 + (\sigma'_Y - \sigma'_z)^2 + (\sigma'_z - \sigma'_x)^2 + 6(\tau'^2_{xy} + \tau'^2_{yz} + \tau'^2_{xz}) = 6k^2 \quad [6]$$

Substituting the values:

$$(\sigma'_x - \sigma'_y)^2 + (\sigma'_y - P_m)^2 + (\sigma'_x - P_m)^2 + 6k^2 = 6k^2 \quad [7]$$

$$(\sigma'_x - \sigma'_y)^2 + (\sigma'_y - P_m)^2 + (\sigma'_x - P_m)^2 = 0 \quad [8]$$

Therefore:

$$\sigma'_x - \sigma'_y = 0$$

$$\sigma'_y - P_m = 0$$

$$\sigma'_x - P_m = 0$$

or

$$\sigma'_x = \sigma'_y = \sigma'_z = P_m \quad [9]$$

Thus, at the onset of bulk plastic flow, the state of stress at the asperity peaks is a combination of simple shear and a hydrostatic pressure, P_m.

Principal stresses are

$$\sigma'_1 = -P_m - k = P'$$

$$\sigma_2 = -P_m + k$$

and

$$\sigma_3 = -P_m \quad [10]$$

If $\bar{a}$ is the average total contact area per unit area of metal surface, and P_{avg} is the average nominal pressure, then:

$$P_{avg} \approx P' \bar{a} \quad [11]$$

The average coefficient of friction is

$$\mu_{avg} \approx \frac{k\bar{a}}{P_{avg}} \quad [12]$$

Using Eq 10 and 11:

$$\mu_{avg} = \frac{k}{P_m + k} \quad [13]$$

Assuming $P_m = 2.9\,\sigma_0$ and $\sigma_0 = \sqrt{3}k$, Eq 13 yields:

$$\mu_{avg} = 0.166 \quad [14]$$

4.2 *Axisymmetric Compression*

In the case of axisymmetric compression, Fig. 3(e) indicates the state of stress acting on an element at the real contact area. σ'_r and σ'_θ are radial and tangential stresses, respectively.

From the discussions:

$$\sigma'_2 = -P_m$$

$$\tau'_{rz} = k$$

and

$$\tau'_{\theta z} = \tau'_{r\theta} = 0$$

Using von Mises yield criteria for secondary asperity deformation yields:

$$\sigma'_\theta = \sigma'_r = \sigma_z = -P_m \quad [15]$$

Thus, P_m is the hydrostatic stress and can be expressed as the mean of the principal stresses:

$$P_m = -\frac{\sigma_1 + \sigma_2 + \sigma_3}{3} \quad [16]$$

where σ_1, σ_1 and σ_3 are the principal stresses.

For yielding:

$$\sigma_2 = \sigma_1 - \sigma_0$$

$$\sigma_3 = \sigma_1 - \sigma_0$$

Therefore:

$$\sigma_1 = -P_m - \frac{2}{3}\sigma_0 = P'$$

$$\sigma_2 = -P_m + \frac{1}{3}\sigma_0$$

and

$$\sigma_3 = -P_m + \frac{1}{3}\sigma_0 \qquad [17]$$

The average friction coefficient is

$$\mu_{avg} = \frac{k}{P_m + \frac{2}{3}\sigma_0} \qquad [18]$$

With $P_m = 2.9\sigma_0$ and $k = \frac{\sigma_0}{\sqrt{3}}$

$$\mu_{avg} = 0.162 \qquad [19]$$

4.3 *Distribution of the Friction Coefficient after Completion of Secondary Asperity Deformation*

As shown in Fig. 5 and 6, the yield pressures at the edge for plane-strain and axisymmetric compressions are equal to $2k$ and σ_0, respectively. The corresponding values of the friction coefficient for full sticking at the edge should therefore be equal to 1/2 and $1/\sqrt{3}$, respectively.

Based on the previous analysis, distribution of the friction coefficient between the center and the edge, after completion of secondary asperity deformation, has been assumed as follows:

For plane-strain compression:

$$\mu = \frac{1}{2}\left(\frac{x}{L/2}\right)^{\alpha} \qquad [20]$$

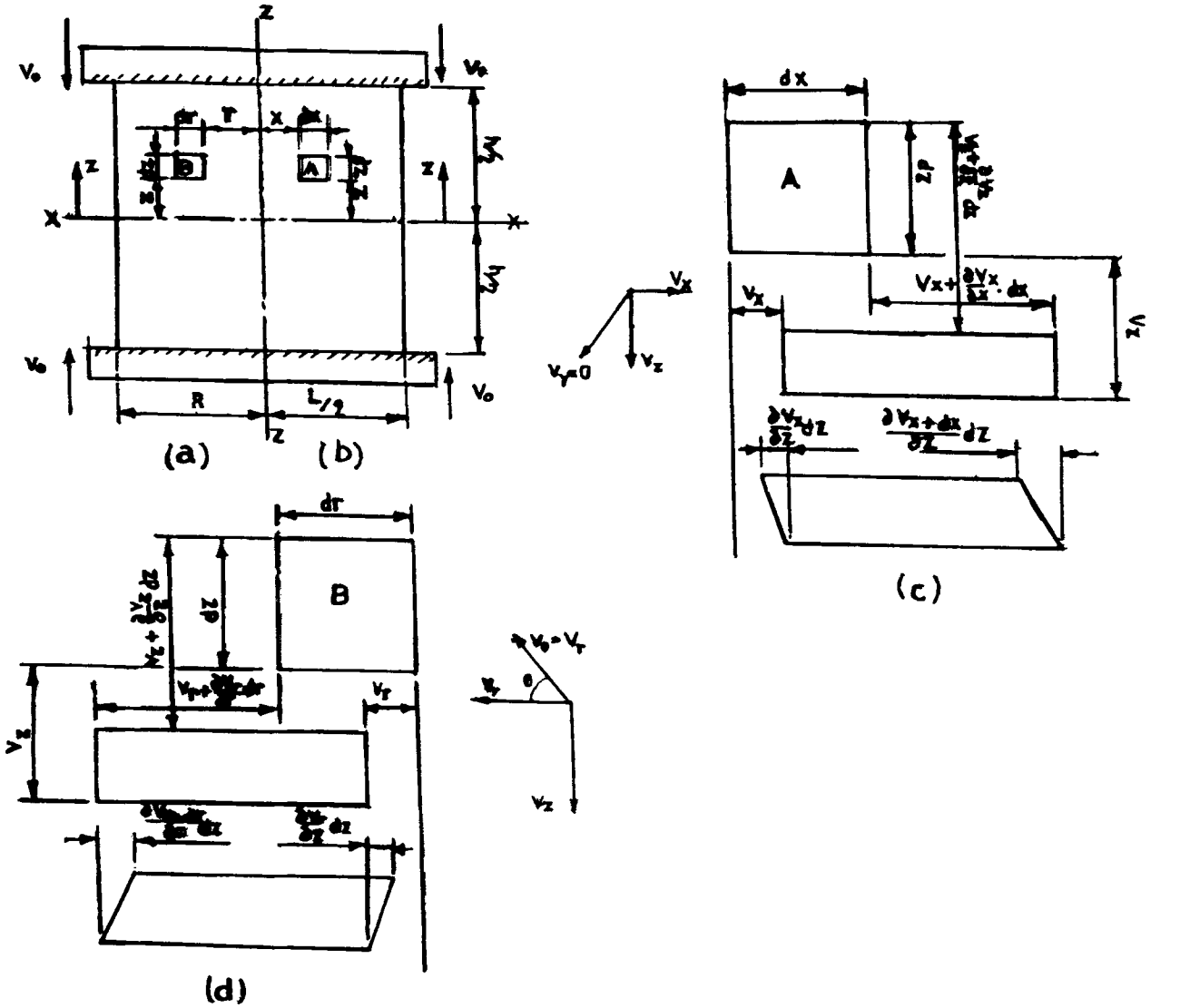

Fig. 7 Deformation and plastic flow for an element undergoing metal compression. Axisymmetric compression (**a** and **d**) and plane-strain compression (**b** and **c**).

For axisymmetric compression:

$$\mu = \frac{1}{\sqrt{3}}\left(\frac{r}{R}\right)^{\beta} \quad [21]$$

where μ is the local friction coefficient, and α and β are the friction exponents assumed in cases of plane-strain and axisymmetric compression, respectively.

In plane-strain compression (Fig. 5), assumed yield criteria at any distance x from the center is

$$P - \sigma_x \cong 2k \quad [22]$$

where σ_x *is the lateral internal stress at a distance x from the center.*

From the equilibrium of forces between $x = 0$ and $x = L/2$ and using Eq 22, one obtains:

$$\int_0^{\frac{L}{2}} \mu P \, dx = \frac{h}{2}(P_o - 2k) \quad [23]$$

where h is the height of the metal specimen, and Po and $2k$ are the local yield pressures at the center and at the edge, respectively.

In case of axisymmetric compression (Fig. 6), the similar equilibrium equation will be

$$\int_0^R \mu P dr = \frac{h}{2}(P_o - \sigma_0) \quad [24]$$

where R is the original radius of the metal specimen, and P_o and σ_0 *are the local yield pressures at the center and at the edge, respectively.*

Because at the onset of bulk deformation the shear stress at the real contact areas reaches the value k, which is the yield stress in pure shear, the magnitude of

$$\int_0^{L/2} \mu P dx$$

or

$$\int_0^R \mu P dr$$

reach a maximum and should remain unchanged at the subsequent stages of compression.

4.4 *Evaluation of Local Average Yield Pressures and the Friction Exponent*

4.4.1 *Plane-Strain Compression*

Referring to Fig. 5, the equilibrium equation of lateral forces on completion of secondary asperity deformation for an element of length dx is:

$$(\sigma_x + d\sigma_x)h - \sigma_x h - 2\mu P dx = 0 \quad [25]$$

Equation 22, after differentiating, yields:

$$d\sigma_x = -dP$$

Also, from Eq 20:

$$\mu = \frac{1}{2}\left(\frac{x}{L/2}\right)^{\alpha}$$

Substituting the values and rearranging, Eq 25 becomes:

$$\frac{dp}{P} = -\frac{1}{h}\left(\frac{x}{L/2}\right)^{\alpha} \quad [26]$$

Integrating and using boundary conditions, Eq. 26 yields:

$$\frac{P}{2k} = \exp\left[\frac{L}{2h(\alpha+1)}\left\{1 - \left(\frac{x}{L/2}\right)^{\alpha+1}\right\}\right] \quad [27]$$

Therefore:

$$\int_0^{\frac{L}{2}} \mu P dx = \frac{h}{2}(P_o - 2k) = hk\left[e^{\frac{L}{2h(\alpha+1)}} - 1\right] \quad [28]$$

With the average coefficient of friction ($\mu_{avg} = 0.166$), Eq 25 in the same manner yields:

$$\int_0^{\frac{L}{2}} \mu P dx = hk\left[e^{0.166\frac{L}{h}} - 1\right] \quad [29]$$

Equating Eq 28 and 29, the value of exponent the α for sticking friction is obtained:

$$\alpha \cong 2.0 \quad [30]$$

Equations 20 and 27 for the local friction coefficient and local yield pressure reduce to:

$$\mu = \frac{1}{2}\left(\frac{x}{L/2}\right)^2 \quad [31]$$

and

$$\frac{P}{2k} = \exp\left[\frac{0.166L}{h}\left\{1 - \left(\frac{x}{L/2}\right)^3\right\}\right] \quad [32]$$

Average pressure at the interface can be evaluated as:

$$\frac{P_{avg}}{2k} = \frac{2}{L}\int_0^{\frac{L}{2}} \exp\left[\frac{0.166L}{h}\left\{1 - \left(\frac{x}{L/2}\right)^3\right\}\right] dx \quad [33]$$

Integrating and neglecting higher order terms, one gets:

$$\frac{P_{avg}}{2k} = 1 + 0.125\left(\frac{L}{h}\right) + 0.0089\left(\frac{L}{h}\right)^2 + 0.00045\left(\frac{L}{h}\right)^3 \quad [34]$$

4.4.2 *Axisymmetric Compression*

Using the slab-force balance method, Eq 21 for the local friction coefficient, μ, and $\mu_{avg}=0.162$, one obtains the following results:

$$b = 2.57 \quad [35]$$

$$\mu = \frac{1}{\sqrt{3}}\left(\frac{r}{R}\right)^{2.57} \quad [36]$$

$$\frac{P}{\sigma_0} = \exp\left[\frac{0.323R}{h}\left\{1-\left(\frac{r}{R}\right)^{3.57}\right\}\right] \quad [37]$$

$$\frac{P_{avg}}{\sigma_0} = 1 + 0.207\left(\frac{R}{h}\right) + 0.026\left(\frac{R}{h}\right)^2 + 0.0024\left(\frac{R}{h}\right)^3 \quad [38]$$

In the same way, it is also possible to evaluate friction exponents and yield pressures at subsequent stages of compression; consequently, it has not been included in the present article.

4.4.3 *Local Friction Factor*

At any point on the die-metal interface, local frictional stress can also be expressed as:

$$\mu P = mk \quad [39]$$

where m is the local friction factor, and therefore:

$$m = 2\mu\left(\frac{P}{2k}\right) \quad [40]$$

Substituting the values from Eq 20 and 32 for plane-strain compression:

$$m = \left(\frac{x}{L/2}\right)^2 \exp\left[\frac{0.166L}{h}\left\{1-\left(\frac{x}{L/2}\right)^3\right\}\right] \quad [41]$$

For axisymmetric compression:

$$m = \sqrt{3}\mu\left(\frac{P}{\sigma_0}\right) \quad [42]$$

or,

$$m = \left(\frac{r}{R}\right)^{2.57} \exp\left[\frac{0.323R}{h}\left\{1-\left(\frac{r}{R}\right)^{3.57}\right\}\right] \quad [43]$$

5. Deformation Kinematics

To propose suitable kinematics of plastic flow in plane-strain and axisymmetric compression, the following assumptions have been made. Velocity discontinuity occurs at every point within the flow field, and deformation takes place symmetrically on both sides of the central axes x - x and z - z (Fig. 7 a and b). Redundant shear stress varies linearly from a maximum at the interface to zero at the midaxis x - x. Boundary conditions for the flow field are as follows.

Plane-strain compression:

$V_x = 0$ when $x = O$ and $z = \pm h/2$
Vx = a maximum when $x = \pm L/2$ and $z = 0$
$V_y = 0$ everywhere
$V_z = V_o$ when $z = \pm h/2$
$V_z = 0$ when $z = 0$

Axisymmetric compression:

$V_r = 0$ when $r = 0$ and $z = \pm h/2$
V_r = a maximum when $r = R$ and $z = 0$
$V_\theta = V_r$ everywhere
$V_z = V_o$ when $z = \pm h/2$
$V_z = 0$ when $z = 0$

Homogenous and redundant deformation models of elements A and B in the cases of plane-strain and axisymmetric compression are shown in Fig. 7 (c) and (d), respectively.

5.1 *Velocity Field*

5.1.1 *Plane-Strain Compression*

As shown in Fig. 7 (b) and (c), velocity components in plane-strain compression satisfying all the boundary conditions are given as:

$$V_x = C\frac{V_o x}{h}\sqrt{1-\frac{z^2}{(h/2)^2}} \quad [44]$$

$$V_y = 0 \quad [45]$$

$$V_z = \frac{2V_o z}{h} \quad [46]$$

where V_o is the uniform velocity of the top and bottom dies, and C is a constant.

From the constancy of volume, the value of C is evaluated as:

$$C = \frac{8}{\pi} \quad [47]$$

Therefore, the expression for V_x becomes:

$$V_x = \frac{8}{\pi}\frac{V_o x}{h}\sqrt{1-\frac{z^2}{(h/2)^2}} \quad [48]$$

5.1.2 *Axisymmetric Compression*

As shown in Fig. 7 (a) and (d), the proposed velocity components for axisymmetric compression satisfying all the boundary conditions and volume constancy are

$$V_r = \frac{4}{\pi}\frac{V_o r}{h}\sqrt{1-\frac{Z^2}{(h/2)^2}} \quad [49]$$

$$V_\theta = V_r \quad [50]$$

$$V_z = \frac{2V_o z}{h} \quad [51]$$

5.2 *Homogeneous Work*

5.2.1 *Plane-Strain Compression*

From Fig. 7(b), the internal work rate for homogenous compression of the element B is determined as:

$$dW_h = 2k\frac{\partial V_z}{\partial z}dz\,dx = 2k\frac{\partial V_x}{\partial x}dx\,dz \quad [52]$$

where $\dot{W}_h$ is the internal work rate for homogeneous compression. Integrating for the entire metal:

$$\dot{W}_h = 4\int_0^{h/2}\int_0^{L/2} 2k\frac{\partial Vz}{\partial z}dz\,dx = 4\int_0^{L/2}\int_0^{h/2} 2k\frac{\partial Vx}{\partial x}dx\,dz \quad [53]$$

or

$$\dot{W}_h = 4kV_o L \quad [54]$$

Equating to the external work rate for homogeneous compression, one obtains:

$$P_h = 2k \quad [55]$$

where P_h is the average homogeneous work pressure.

5.2.2 *Axisymmetric Compression*

In axisymmetric compression, the internal work rate for homogeneous compression and the average homogenous work pressure can be obtained in the same manner:

$$W_h = 2\pi R^2 \sigma_0 V_o L \quad [56]$$

and

$$P_h = \sigma_0 \quad [57]$$

5.3 *Redundant Work*

5.3.1 *Plane-Strain Compression*

Redundant shear stress at any point within the flow field is

$$\tau = mk\frac{2z}{h} \quad [58]$$

Substituting the value of m from Eq 41 yields:

$$\tau = \frac{2kz}{h}\left(\frac{x}{L/2}\right)^2 \exp\left[\frac{0.166L}{h}\left\{1-\left(\frac{x}{L/2}\right)^3\right\}\right] \quad [59]$$

From Fig. 7(b), the redundant work rate for the element A is

$$d\dot{W}_r = \tau\frac{\partial V_x}{\partial z}dz\,dx \quad [60]$$

where $\dot{W}_r$ is the redundant work rate.

From Eq 48:

$$\frac{\partial V_x}{\partial z} = -\frac{32}{\pi}\frac{V_o x}{h^3}\frac{z}{\sqrt{1-\frac{z^2}{(h/2)^2}}} \quad [61]$$

Substituting the values of τ and $\frac{\partial V_x}{\partial z}$ in Eq 60, from Eq 59 and 61, respectively, and integrating for the entire volume, $\dot{W}_r$ is obtained. Neglecting the higher order terms:

$$\dot{W}_r = 4kV_o L\left[0.125\left(\frac{L}{h}\right)+0.0089\left(\frac{L}{h}\right)^2+0.00045\left(\frac{L}{h}\right)^3\right] \quad [62]$$

Equating to the external work rate for redundant deformation, one obtains:

$$\frac{P_r}{2k} = 0.125\left(\frac{L}{h}\right)+0.0089\left(\frac{L}{h}\right)^2+0.00045\left(\frac{L}{h}\right)^3 \quad [63]$$

where P_r is the average redundant work pressure.

5.3.2 *Axisymmetric Compression*

In axisymmetric compression, the redundant work rate for the element B is

$$d\dot{W}_r = \tau\, r\, d\theta\, dr\frac{\partial V_r}{\partial z}dz \quad [64]$$

So,

$$\dot{W}_r = 2\pi R^2 \sigma_0 V_o\left[0.207\left(\frac{R}{h}\right)^2+0.026\left(\frac{R}{h}\right)^2\left[+0.0024\left(\frac{R}{h}\right)^3\right]\right] \quad [65]$$

Equating to the external work rate for redundant deformation, one obtains:

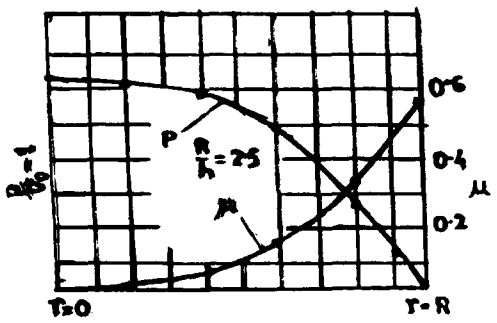

Fig. 8 Local yield pressures and friction coefficients (calculated) in axisymmetric compression.

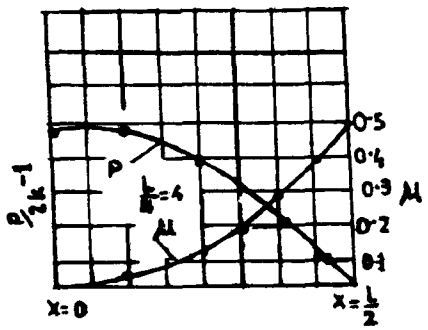

Fig. 9 Local yield pressures and friction coefficients (calculated) in plane-strain compression.

$$\frac{P_r}{\sigma_0} = 0.207\left(\frac{R}{h}\right) + 0.026\left(\frac{R}{h}\right)^2 + 0.0024\left(\frac{R}{h}\right)^3 \qquad [66]$$

5.3.3 *Average Total Pressure*

Average total pressure, P_{avg}, is

$$P_{avg} = P_h + P_r \qquad [67]$$

Therefore, in plane-strain compression:

$$\frac{P_{avg}}{2k} = 1 + 0.125\left(\frac{L}{h}\right) + 0.0089\left(\frac{L}{h}\right)^2 + 0.00045\left(\frac{L}{h}\right)^3 \qquad [68]$$

In axisymmetric compression:

$$\frac{P_{avg}}{\sigma_0} = 1 + 0.207\left(\frac{R}{h}\right) + 0.026\left(\frac{R}{h}\right)^2 + 0.0024\left(\frac{R}{h}\right)^3 \qquad [69]$$

6. Comparison of Results

For the purpose of comparison, local yield pressures and friction coefficients at various points on the die-metal contact have been evaluated for specific R/h and L/h ratios, using the derived formulas (Eq 32 and 37). The results have been plotted and shown in Fig. 8 and 9, respectively. The distribution pattern of local yield pressures between the center and the edge are found to be well in agreement with the experimental curve shown in Fig. 10.[4].

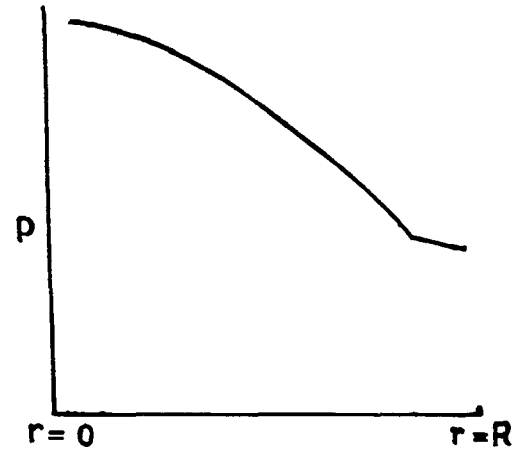

Fig. 10 Distribution of local pressures (actual) in axisymmetric compression with sticking friction. [1,4]

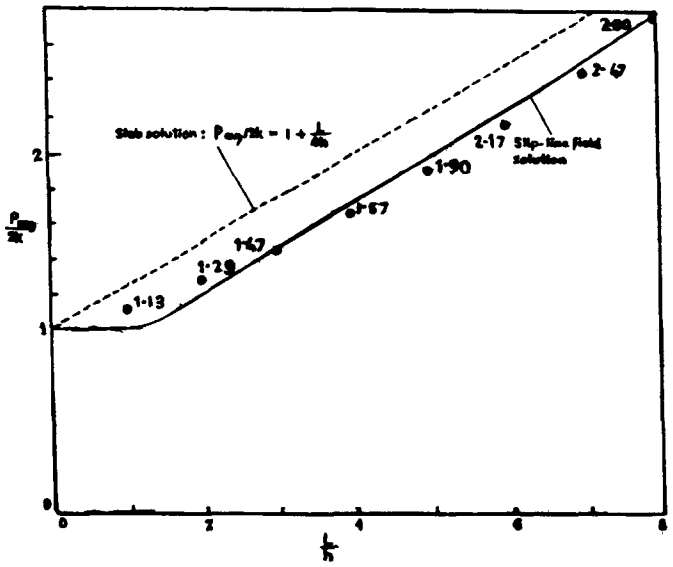

Fig. 11 $P_{avg}/2k$ versus L/h for plane-strain compression.

It may be seen from the analysis that the expressions for $P_{avg}/2k$ or P_{avg}/σ_0 derived by the upper bound slab-energy method (Eq 68 and 69) are identical to those obtained using the slab-force balance method (Eq 34 and 38). Also, the values of $P_{avg}/2k$ for different L/h ratios have been evaluated and plotted against the corresponding slip-line field solutions in Fig. 11. All of these values are observed to be extremely close to the respective slip-line field results.

7. Conclusions

From the analysis in the preceding pages, the following conclusions can be drawn. In metal compression, asperities on the metal surface deform in two stages. Whereas, the primary asperity collapse occurs under normal loading before the onset of gross deformation, the secondary deformation and junction growth begins with the start of gross plastic flow. Bulk plastic deformation has a strong influence on the interface frictional characteristics. Complete strain transfer takes place at the interface surface layer. Although tensile strain, as in the case of stretch forming of sheet metal, reduces the asperity collapse pressure, compressive strain in metal compression increases the pressure. The increase in asperity collapse pressure in cases of plane-strain and axisymmetric compression are equal to k and $2/3\ \sigma_0$, respectively.

At the onset of bulk plastic flow, local frictional characteristics at any point on the metal surface are dependent on the initial surface topography. However, it is possible to evaluate average coefficients of sticking friction in plane-strain and axisymmetric compression as 0.166 and 0.162, respectively. Subsequent to complete strain transfer to the interface, full sticking occurs at and near the edge of the metal specimen, and the frictional stresses progressively lessen toward the center. At the edge, the friction coefficient is the highest, whereas at the center it is zero. The approximate values of the friction exponents showing distribution of the friction coefficients between the edge and the center, for plane-strain and axisymmetric compression, are 2.0 and 2.57, respectively.

Plastic flow kinetics, as proposed in the current article, assume velocity discontinuity at every point within the deformation zone and assume that a dead metal cap does not exist inside the flow field. At the interface, the metal sticks to the die surface, and no micro- or gross sliding takes place there.

Using the derived frictional characteristics and the proposed velocity field, both the slab-energy method and the slab-force balance method yield identical expressions for average yield pressures. The calculated results are found to be extremely close to the corresponding slip-line field solutions. The proposed interface sticking friction and plastic flow kinematics in metal compression are therefore valid and more realistic compared to earlier assumptions.

Acknowledgment

The author is thankful to Mr. K.K. Majumder, MECON, for helping him write the paper. He also expresses his gratitude to Mrs. B. Mukherjee for typing the manuscript.

References

1. W.F. Hosford and R.M. Caddell, *Metal Forming Mechanics and Metallurgy*, Prentice-Hall, Englewood Cliffs, (1983).
2. R.M. Caddell and W.F. Hosford, *Int. J. Mech. Eng., 8*, 1-6 (1980).
3. W. Johnson and P.B. Mellor, *Plasticity for Mechanical Engineers*, D. Van Nostrand, New York (1962).
4. G.E. Dieter, *Mechanical Metallurgy*, 2nd ed., McGraw-Hill, New York (1976).
5. G.W. Rowe, *Elements of Metal Working Theory*, Edward Arnold Ltd., London (1979).
6. G.T. Van Rooyen and W.A. Backofen, *J. Mech. Phys. Solids, 7*, 163-168 (1959).
7. G.W. Pearsall and W.A. Backofen, *Trans. ASME B*, 68-75 (1963).
8. A. Nadai, *Theory of Flow and Fracture of Solids*, Vol I, 2nd ed., McGraw-Hill, New York (1950).
9. W.L. Roberts, *Hot Rolling of Steel*, Marcel Dekker, New York (1983).
10. A.K.E.H.A. El-Kalay and L.G.M. Sparling, Factors Affecting Friction and their Effect upon Load, Torque and Spread in Hot Flat Rolling, *J. Iron Steel Inst.*, Feb, 152-163 (1968).
11. R.B. Sims, Calculation of Roll Force and Torque in Hot Rolling Mills, *Proc. Inst. Mech. Eng., 168*, 191-219 (1954).
12. H. Ford and J.M. Alexander, Simplified Hot Rolling Calculations, *J. Inst. Metals, 92*, 397-403 (1963-64).
13. F.A.A. Crane and J.M. Alexander, Slip Line Fields and Deformation in Hot Rolling of Strips, *J. Inst. Metals, 96*, 289-300 (1968).
14. W.L. Roberts, Computing the Coefficient of Friction in the Roll Bite from Mill Data, *Blast Furnace and Steel Plant*, 499-508 Jun (1967).
15. J.F. Archard, *Proc. Roy. Soc. Ser. A, 243*, 190 (1957).
16. J.A. Greenwood and J.B.P. Williamson, *Proc. Roy. Soc. Ser. A, 295*, 300 (1966).
17. D.J. Whitehouse and J.F. Archard, *Proc. Roy. Soc. Ser. A, 316*, 97 (1970).
18. J. Pullen and J.A. Greenwood, *Proc. Roy. Soc. Ser. A, 327*, 159 (1962).
19. F. Ling and N.Y. Troy, *Trans. ASME, 80*, 1113 (1958).
20. T.H.C. Childs, *Proc. Roy. Soc. Ser. A, 353*, 35 (1977).
21. T. Wanheim and N. Bay, *CIRP Ann., 27* (1978).
22. J. Halling, *Introduction to Tribology*, Wykeham (1975).
23. J.A. Greenwood and J.B.P. Williamson., *Proc. 4th Leeds - Lyd Symp. Tribology*, Institute of Mechanical Engineering, 167-177 (1978).
24. F.P. Bowden and D. Tabor, *Friction and Lubrication of Solids, Part I*, Oxford University Press (1964).
25. D. Tabor, *Proc. Roy. Soc., Ser A, 251*, 378 (1959).
26. H. Kaga and Yaji, *Proc. 12th Jpn. Cong. Metall. Res.*, 165 (1969).
27. P.F. Thompson and P.V. Nayak, *Int. J. Mach. Tool Des. Res., 20*, 73 (1980).
28. B. Fogg, *Proc. I. Mech. E., 182*, 152 (1968).
29. A.K. Sengupta, B. Fogg, and S.K. Ghosh, On The Mechanism Behind the Punch-Blank Surface Conformation in Stretch Forming and Deep Drawing, *J. Mech. Work. Tech., 5*, 181-210 (1981).